Electronic Supplementary Material (ESI) for Nanoscale.

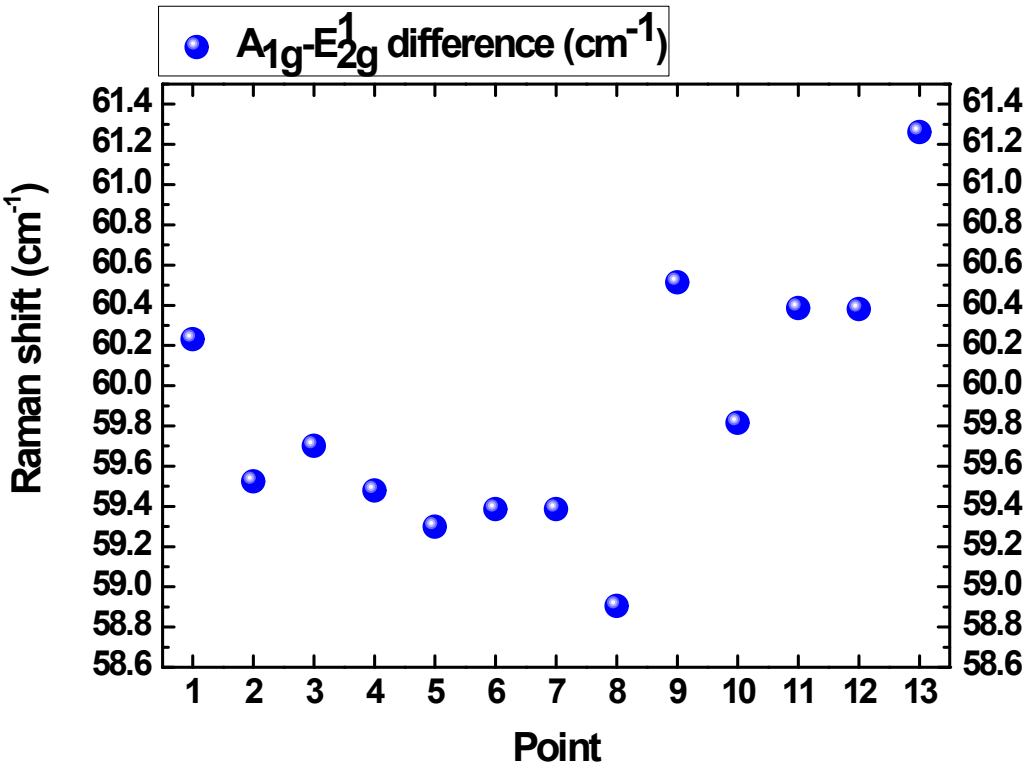

FIG.S1. Energy difference between the two most prominent Raman vibrational modes, E_{2g}^1 (in plane) and A_{1g} (out of plane), for the 13 different points of the WS_2 monolayer. This difference is ranging from 58.8 cm^{-1} to 61.3 cm^{-1}.

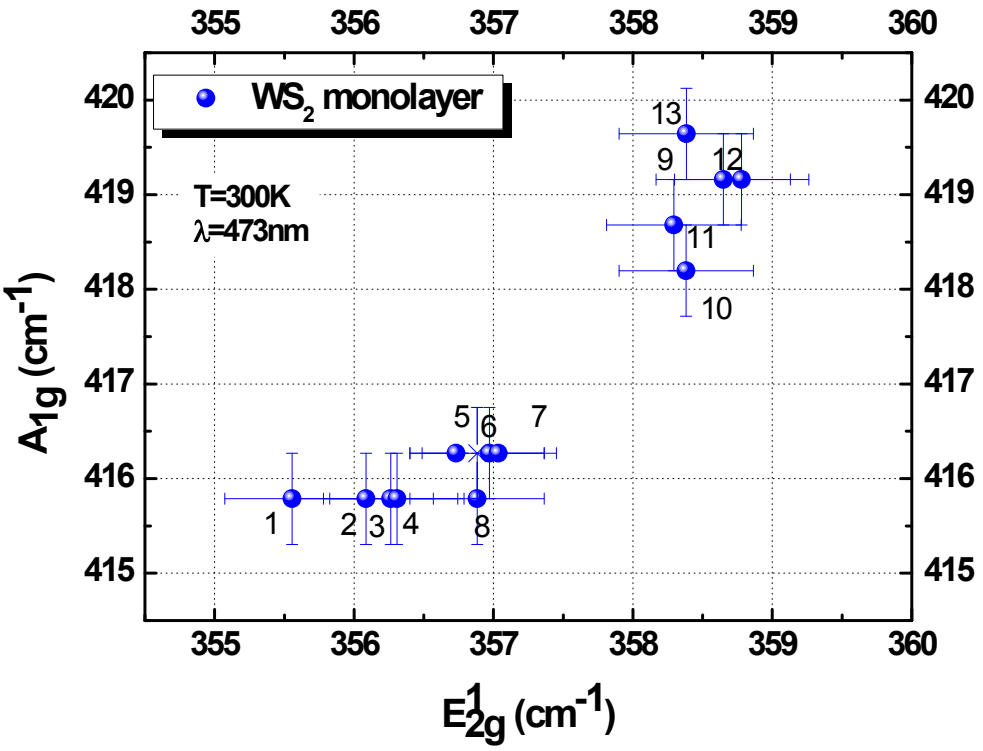

F

IG.S2. Energy of A_{1g} as a function of the energy of E^1_{2g}, for all the different points measured. Differences ranging from 0.5 cm^{-1} (resolution limit) to a maximum of 4 cm^{-1} for the A_{1g} mode and 3.2 cm^{-1} for the E^1_{2g} mode, can be observed. Two different groups of points can be distinguished (1 to 8 and 9 to 13) suggesting strain heterogeneity across the monolayer's area.

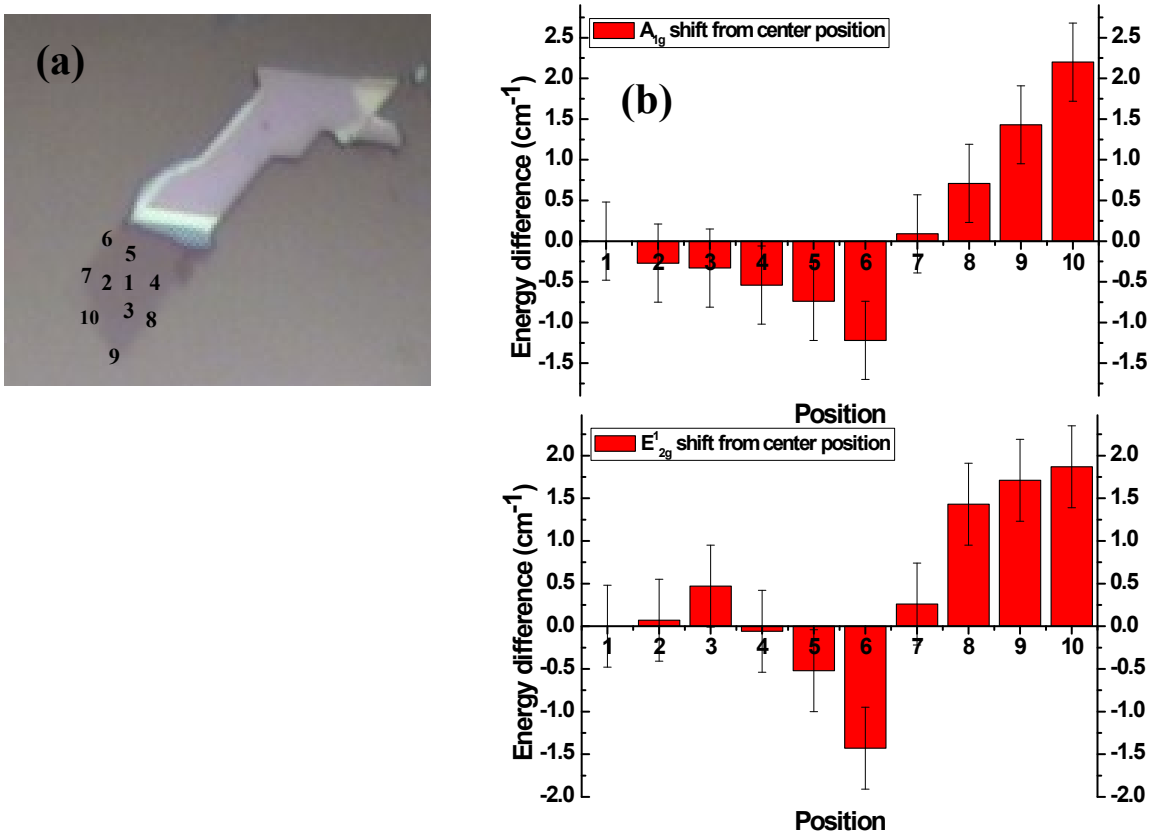

FIG.S3. (a) Optical microscopy image of a WS2 monolayer, where different positions (from 1 to 10) used to obtain Raman spectra are indicated. Specifically, number 6 to 10 represent the edge regions of the single layer and numbers 1 to 5 are located in the inner area. (b) Raman shifts of the different areas with respect to position 1 that is located in the center of the monolayer.

In order to confirm that the observations of Fig. 2 regarding the partial oxidation of the edge of the ML WS_2 we repeated the SAM/AES analysis to second sample, as shown in Fig. S4. SEM and SAM revealed an area between the bulk and ML WS_2, where the sample is completely detached (dark area in SEM, cyan area in SAM). After identifying the extent of ML WS_2 by SEM we acquired AES spectra at points A, B and C that correspond to bulk WS_2, the center of monolayer WS_2 and the edge of the monolayer WS_2, respectively. The shift of the principal W_{MNN} peak to lower kinetic energy, indicating the oxidation of W, is also clearly observed for this second sample.

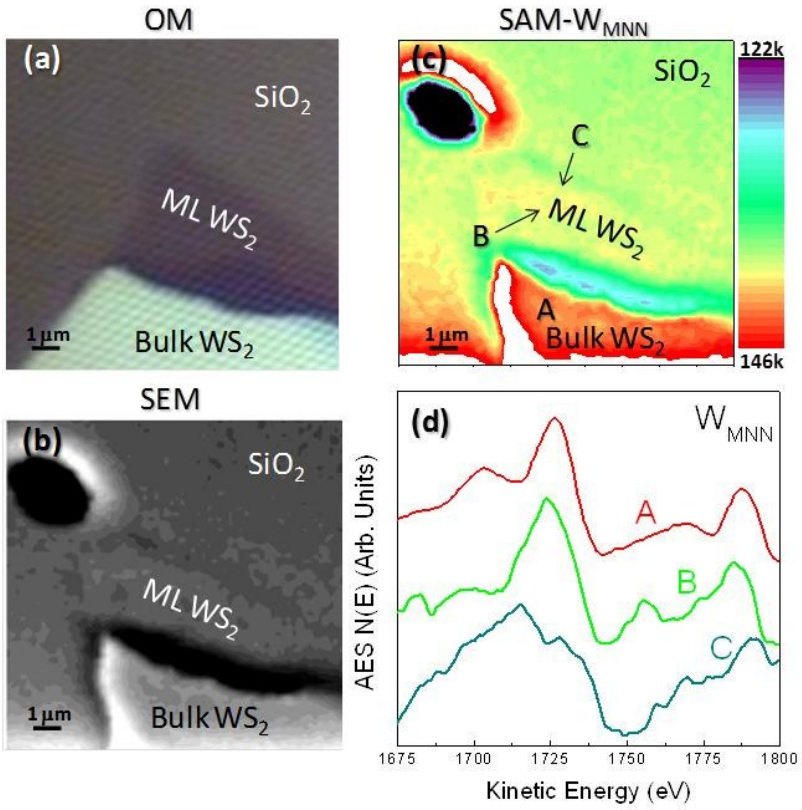

FIG.S4. (a) Optical microscope image of a WS_2 crystal (bright area) with a WS_2 monolayer extended beyond the crystal (dark shadowed area), (b) SEM image from the same area where the ML WS_2 is better resolved, (c) the surface distribution of W in the

same region acquired by SAM recording the W_{MNN} peak strength; A, B, and C are the points where AES spectra have been measured (and correspond to bulk WS_2, the center of monolayer WS_2 and the edge of the monolayer WS_2), (d) W_{MNN} AES spectra from points A, B and C.

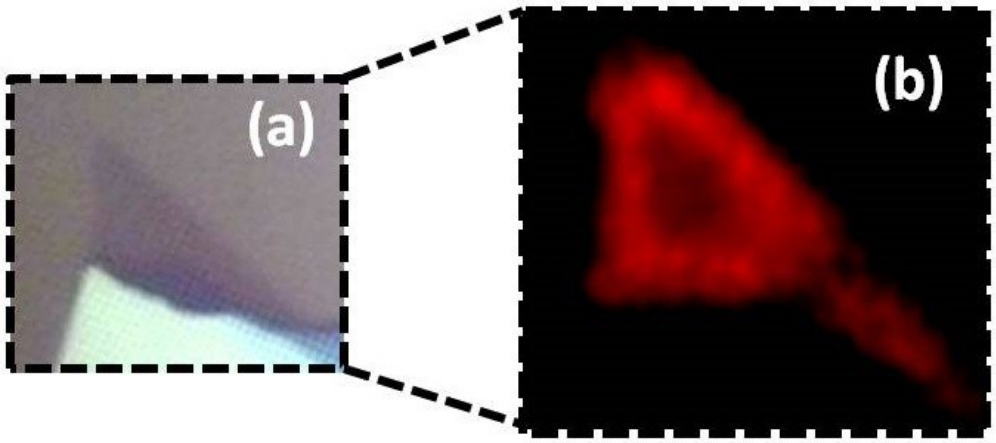

FIG.S5. (a) Typical optical microscopy image of exfoliated WS_2 monolayer of Fig. S4. (b) Fluorescence image of WS_2 monolayer using a spatially homogeneous 543nm He-Ne laser beam.

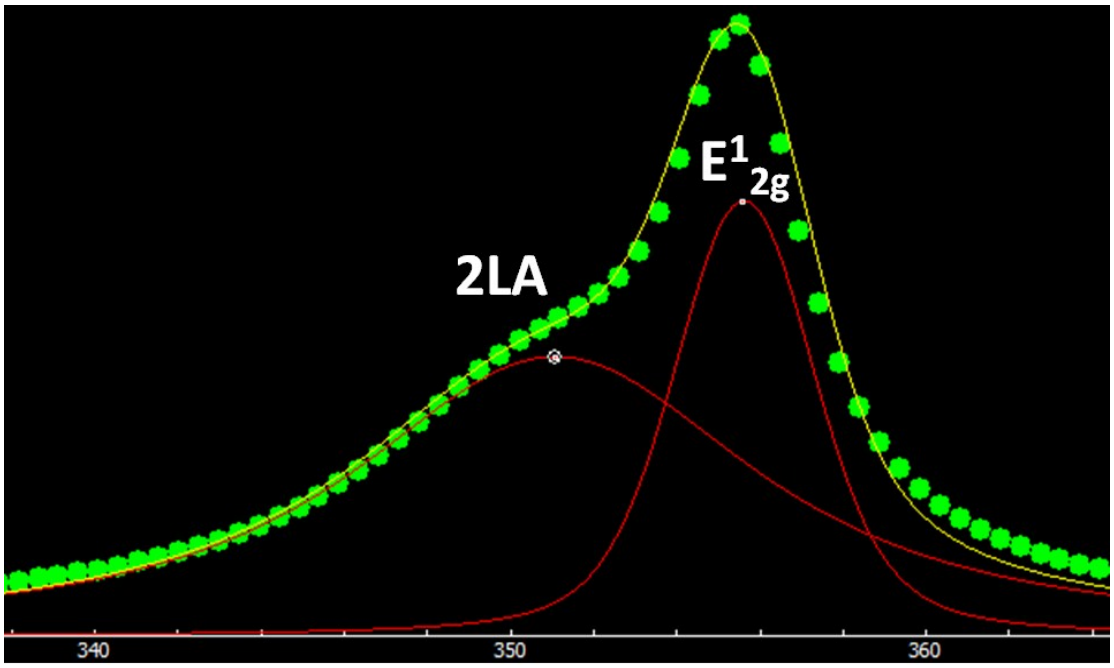

FIG.S6. Fitting result of E^1_{2g} and 2LA modes. The green spots correspond to the experimental data, red curves represent the voigt function of each mode and yellow line is the sum of the two functions.